

Channel Estimation, Interference Cancellation, and Symbol Detection for Communications on Overlapping Channels

Minh Tri Nguyen and Long Bao Le

INRS, University of Quebec, Montreal, QC, Canada. E-mails: {minh.tri.nguyen, long.le}@emt.inrs.ca

Abstract—In this paper, we propose the joint channel estimation, interference cancellation, and data symbol detection for unsynchronized communications of different bandwidths over overlapping channels. To this end, we have to estimate the Effective Interference Coefficients (EICs) and the desired channel coefficients. We construct a two-phase framework where the EICs and desired channel coefficients are estimated using the maximum a posteriori probability (MAP) criteria in the first phase and the MAP based data symbol detection is performed in the second phase. We analyze the channel estimation error, residual interference, symbol error rate (SER) achieved by the proposed framework. We then discuss how to optimize the pilot density to achieve the maximum throughput. Via numerical studies, we show that our design can effectively mitigate the interference for a wide range of SNR values and our proposed channel estimation and symbol detection design can achieve better performance than the existing method.

Index Terms—Interference cancellation, fast fading, symbol detection, and channel estimation.

I. INTRODUCTION

Traffic demand from wireless networks has been increasing dramatically over the last decades while spectrum resource is limited. This has motivated the development of efficient and flexible spectrum utilization and sharing techniques for wireless communications. Moreover, future wireless networks are expected to support a massive number of connections to enable many emerging applications requiring diverse communication rates and quality of service [1]. Therefore, effective spectrum reuse using robust interference cancellation and management is essential in maintaining and enhancing the communication rate and reliability in next-generation wireless systems [2]. In particular, future wireless systems are expected to support different applications and use cases, e.g., highly mobile scenarios in which users move at high speeds (up to 500 km/hr) [3]–[5] and communications over very fast fading channels [6]–[8].

In many emerging use cases, co-channel wireless interference can be very strong which requires advanced and robust interference cancellation techniques. Full-duplex (FD) communication is one such scenario [9] where the combined analog and digital interference cancellation strategies are typically employed to achieve sufficient cancellation performance [10]. In fact, FD communication has a special interference structure where the interfering and interfered communications have the same bandwidth (hence, the same symbol rate), which plays a

crucial role in designing interference cancellation techniques, especially in the digital domain [11], [12]. Interference cancellation for the scenario where interfering source and victim have different bandwidths is more challenging. This is because the equivalent interference coefficients (EICs) [13] vary from symbol to symbol and the concurrent communications are likely not synchronized [14].

Different interference cancellation methods have been developed for FD wireless systems over the last few years, including passive interference cancellation [15] and active interference cancellation in the analog domain [16], [17] or in the digital domain [11], [12]. Even though various interference cancellation techniques have been proposed for full-duplex systems, only a few works study interference cancellation for the concurrent communications with different symbol rates. Thus, development of robust interference cancellation methods that can effectively address a general interference scenario between two communications of different bandwidths is highly important [18].

In the high mobility environment, it is more challenging to accurately estimate, track, or predict the fast time-varying fading channels. This is especially critical because the data detection performance depends on the interference cancellation and channel estimation quality. As a result, channel estimation errors must be typically jointly designed with data detection. The commonly adopted assumption of perfect channel state information (CSI), which could be partly justified in the low mobility environment, would no longer be valid for high mobility systems. Thus, it is highly desirable to develop robust techniques that can cope with the combined challenges of strong interference and fast fading.

Interference cancellation for communications with different bandwidths has been carried out in some previous works [13], [19] assuming perfect CSI and/or synchronization between the underlying communications. The problem becomes much more challenging when the desired channel experiences fast fading where the time-varying channel can be modeled by using the first-order Gauss-Markov process [7], [20]–[22]. For the fast fading channel, MMSE-based channel estimators are derived in [23], [24], which requires the knowledge of the channel correlation matrix, which may not be readily usable in the presence of interference. Moreover, the MMSE-based estimation method typically requires large matrix inversion,

which therefore has high computational complexity.

For the interference scenario with fast fading, channel estimation and interference mitigation using the message-passing approach is considered to estimate the posterior probability of data symbols [25]. However, this proposed method only works well if the interfering and desired signals are synchronized and have the same symbol rate. Furthermore, an approximated distribution of data symbols by the Gaussian mixture with a limited number of terms may yield unacceptable error rate with a large signal constellation size.

The aforementioned survey of existing literature suggests that joint channel estimation, interference cancellation, and symbol detection for the scenario with two un-synchronized interfering signals having different communication bandwidths over the fast fading channel has been underexplored. This paper aims to fill this gap in the literature and makes the following contributions.

- 1) A two-phase framework for joint estimation of EICs, fast-fading channel coefficients, and symbol detection is proposed. In the first phase, the EICs are estimated and the interference is subtracted from the received signal, then fast-fading channel coefficients at pilot positions are estimated. In the second phase, the symbols' *a posteriori probability* is derived given the channel coefficients at the pilot positions to enable symbol detection. Specifically, we consider both series and individual symbol detection methods and derive the corresponding a posteriori probabilities for both methods.
- 2) We then analyze the residual interference and symbol error rate achieved by the proposed design. Specifically, we provide an exact expression for channel estimation error in the interference-free scenario, and an approximated residual interference and channel estimation error for the case with interference. The analysis shows that the residual interference has bounded power as the interference power tends to infinity. However, the effect of the fast fading channel to the residual interference is irreducible no matter how large the SNR or the number of pilot symbols is. Hence, there are fundamental floors for the channel estimation and symbol detection performances.
- 3) We conduct simulation studies and draw several insightful observations from the numerical results. Particularly, the performance floor exists for the considered interference scenario while it is not the case for the interference free scenario. The series symbol detection outperforms the existing detection method in terms of SER while the individual symbol detection achieves very close (almost identical) performance to the existing detection method but with much lower complexity. Finally, we show that there exists an optimal frame structure (i.e., optimal pilot density) to achieve the maximum system throughput.

While preliminary results of this paper were published in [26], the current paper makes several significant contributions compared to this conference version. Specifically, the con-

ference version only considered the series symbol detection method while the current journal paper studies two detection methods. The theoretical performance analysis and throughput optimization were not performed in the conference version. Moreover, the current journal paper presents much more extensive numerical results which provide useful insights into the proposed design.

The paper is structured as follows. The system model and problem formulation are presented in Section II. Section III describes the proposed channel estimation, interference cancellation, and the symbol detection techniques. In Section IV, we analyze the residual interference, SER, and optimal frame design for the fast fading and interference scenario. Numerical results are presented in Section V and Section VI concludes the paper.

Some important notations used in the paper are summarized as follows: \mathbf{I}_N represents the $N \times N$ identity matrix, $\mathbf{1}_{M,N}$ is the $M \times N$ all-one matrix, \mathbf{A}^H is the *Hermitian transpose* of matrix \mathbf{A} , x^* is the *conjugate* of complex value x , $\mathbb{1}_{i=j}$ is the indicator function equal to one when $i = j$ and equal to zero otherwise, *const.* represents a constant independent of the variables of interest, (\star) denotes the convolution operation and (\propto) denotes '*proportional to*'.

II. SYSTEM MODEL AND PROBLEM STATEMENT

We consider the scenario where two communication links denoted by \mathbf{S}^d (desired link) and \mathbf{S}^i (interfering link) operate on overlapping frequency bands. The transmitted signal from \mathbf{S}^i interferes with the received signal of \mathbf{S}^d . One popular assumption usually made in the literature is that interfering and desired signals have identical bandwidths where the full-duplex system is a special setting attracting great interests recently. Our current paper considers the more general scenario in which the frequency bands of the two communication links can be arbitrarily aligned and their bandwidth ratio is an integer.

We further assume that the desired communication channel experiences the fast fading where the channel coefficient changes from symbol to symbol according to the first order Markov process [20], [27]. In addition, the interfering channels from the interfering source to the antennas of desired receiver is assumed to be line of sight. In this interference scenario, the involved signals have different bandwidths and are not synchronized with one another. This induces a dynamic interference pattern for desired received symbols, which can be captured by the EICs [13], [19]. We propose to jointly estimate the desired channel coefficient and EICs with the knowledge of transmitted symbols from the interfering source and pilots transmitted from the desired transmitter.

A. Signal Model

The transmitted signal of the desired communication having carrier frequency f^d can be written as

$$s^d(t) = \sum_{k=-\infty}^{\infty} x_k p^d(t - kT^d + \epsilon^d) e^{j(2\pi f^d t + \theta^d)}, \quad (1)$$

where x_k is the k th transmitted symbol. The pulse shaping function $p^d(t)$ has unity gain; T^d , ϵ^d and θ^d represent the symbol duration, time and phase offsets, respectively. Similarly, the signal from the interfering source can be written as

$$s^i(t) = \sum_{k^i=-\infty}^{\infty} b_{k^i} p^i(t - k^i T^i - t^i) e^{j(2\pi f^i t + \theta^i)}, \quad (2)$$

where $p^i(t)$ denotes the pulse shaping filter with unity gain, the interfering signal has the center frequency $f^i = f^d - \Delta f$, the k^i th symbol is b_{k^i} ; t^i and θ^i account for the time/phase difference of the two systems and transmission time delay from the interfering transmitter to the interfered receiver, respectively. Assume that there are N_r receiver antennas for \mathbf{S}^d , then the received signal is

$$\mathbf{y}(t) = \mathbf{h}^d(t) \star s^d(t) + \mathbf{h}^i(t) \star s^i(t) + \mathbf{w}(t), \quad (3)$$

where $\mathbf{h}^d(t)$ and $\mathbf{h}^i(t)$ denote $N_r \times 1$ vectors of desired and interfering channel impulse responses.

At the receiver of \mathbf{S}^d , the signals are down-converted to baseband by using $e^{-j(2\pi f^d t + \theta^d)}$. The output signals then pass through a matched filter having the impulse response $p^d(t)$; and the filtered continuous signals are sampled at $(kT^d + \epsilon^d)$ to yield the following discrete time signal

$$\mathbf{y}_k = \mathbf{h}_k^d x_k + \mathcal{I}_k + \mathbf{w}_k, \quad (4)$$

where \mathbf{w}_k represents the vector of noise having complex Gaussian distribution with covariance matrix $\sigma^2 \mathbf{I}_{N_r}$ (called AWGN hereafter for short); \mathcal{I}_k denotes the equivalent baseband, discrete time interfering signal which will be derived shortly. Firstly, we express the interference terms in the continuous time domain as follows:

$$\mathcal{I}(t) = \left\{ (\mathbf{h}^i(t) \star s^i(t)) e^{-j(2\pi f^d t + \theta^d)} \right\} \star p^d(t). \quad (5)$$

Substituting $s^i(t)$ from (2) into (5), we obtain the equivalent baseband interference signal whose sampled signal at time $(kT^d + \epsilon^d)$ is

$$\mathcal{I}_k = \mathcal{I}(t)|_{t=kT^d + \epsilon^d} = \mathbf{h}_k^i \sum_{k^i} b_{k^i} c_{k,k^i}, \quad (6)$$

where c_{k,k^i} represents the EIC which is defined in (7).

B. Channel Model

The fast fading channels of the desired communication link \mathbf{h}_k^d in (4) follow the first-order Markov model where the relation of channel coefficients at instants $(k+1)$ th and k th can be described as [20], [25]:

$$\mathbf{h}_{k+1}^d = \alpha \mathbf{h}_k^d + \sqrt{1 - \alpha^2} \mathbf{\Delta}_k, \quad (8)$$

where $\mathbf{\Delta}_k$ denotes a vector of Circular Symmetric Complex Gaussian (CSCG) noise with zero means and covariance matrix $\sigma_h^2 \mathbf{I}_{N_r}$. The additive noise term in (8) is called channel evolutionary noise and α is the channel correlation coefficient. The average Signal to Noise Ratio (SNR) is $\rho = \sigma_h^2 / \sigma^2$ (called SNR without fading in some previous works [23]). Without loss of generality, we let $\sigma_h^2 = 1$. However, σ_h^2 may appear occasionally in several expressions whenever needed.

C. Problem Statement

For the considered interference scenario where the bandwidth of the interfering signal is multiple times larger than that of the desired signal, several symbols of the interfering signal will affect each desired symbol during its symbol interval. Suppose that the interfering signal's bandwidth is M times larger than that of the interfered signal's bandwidth and there are L symbols of b_{k^i} 's interfering to each desired symbol x_k where L should be a multiple of the bandwidth ratio to account for the interference in the filter span of the desired signal. Since the bandwidth ratio is an integer, c_{k,k^i} in (7) depends only on the relative difference of k, k^i . For brevity, we denote them as $\{\mathbf{c} = [c_1, c_2, \dots, c_L]^T\}$ in the sequel. We assume that the receiver has the information about the interfering channel gains $\mathbf{h}_k^{i,1}$. Using the result of \mathcal{I}_k in (6), we can rewrite the received signal as

$$\begin{aligned} \mathbf{y}_k &= \mathbf{h}_k^d x_k + \mathbf{h}_k^i \sum_{l=1}^L c_l b_{Mk+l} + \mathbf{w}_k \\ &= \mathbf{h}_k^d x_k + \mathbf{B}_k \mathbf{c} + \mathbf{w}_k, \end{aligned} \quad (9)$$

where \mathbf{B}_k represents the $N_r \times L$ known overall interference matrix whose j -th column is $\mathbf{h}_k^i b_{Mk+j}$. In this paper, \mathbf{y}_k is referred to as the *received signal* or *observation* interchangeably. Since the interfering channels are known and captured in the interference matrix \mathbf{B}_k , we will omit the superscript d in the desired channel notation, i.e., \mathbf{h}_k^d becomes \mathbf{h}_k . From now on, *channels* means desired channels discussed in the previous sections.

This paper aims to address the following questions:

- 1) Given the interference matrix \mathbf{B}_k , the observations \mathbf{y}_k and the pilot symbols, how one can cancel the interference and detect data symbols reliably?
- 2) What are the effects of fast fading channel evolutionary noise to the overall system performances (EIC estimation, interference cancellation, and channel estimation)?
- 3) Is there an optimal frame design (i.e., optimal pilot density) that maximizes the throughput in the presence of fast fading and interference?

In the next sections, we will provide the answers for these questions.

III. PROPOSED CHANNEL ESTIMATIONS AND INTERFERENCE CANCELLATION STRATEGY

Even though the MMSE method has been widely used in channel estimation, this method relies heavily on the knowledge of the time-domain channel correlation [24], [28]–[30]. In the presence of interference, MMSE can only be applied after the interference is canceled out. Moreover, its achieved performance depends on the interference cancellation techniques and the resulted residual interference. In addition, MMSE estimators typically require matrix inversion having high complexity with respect to (w.r.t.) number of pilot symbols, which may become unaffordable for long frames. These

¹The interfering channel gains correspond to the line of sight link as described. Therefore, they can vary slowly over time and can be estimated accurately.

$$c_{k,k^i} = \int_{-\infty}^{\infty} p^d(kT^d + \epsilon^d - \tau) p^i(\tau - k^i T^i - t^i) e^{j(2\pi(f^i - f^d)\tau + \theta^i + \theta^d)} d\tau. \quad (7)$$

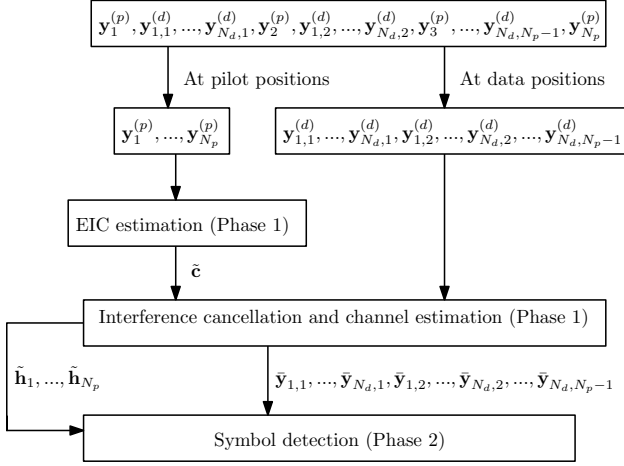


Fig. 1: Illustration of the proposed design

drawbacks of the MMSE method motivate us to consider the MAP estimator instead. Furthermore, the MAP estimator is usually preferable to other estimation techniques in terms of both bias and variance for the setting with a small number of observations, which corresponds to the small number of pilot symbols in our considered data frame [31].

In this section, we propose a two-phase design framework for estimation of channel effective interference coefficients and symbol detection. In the first phase, the EICs are estimated at each pilot position using the maximum likelihood (ML) approach. Then, we take the average of the estimates of \mathbf{c} over all pilot positions to obtain a reduced-variance estimate of \mathbf{c} compared to its estimates at different pilot positions. After that the interference is subtracted from the received signal and the channel coefficients are estimated at pilot positions. In the second phase, the maximum a posteriori of data symbols is derived, given estimated channel coefficients at pilot positions before and after data intervals. Fig. 1 illustrates our proposed receiver structure for one particular frame.

Channel estimation and data detection are performed in each frame. We consider the scattered pilot structure with N_d data symbols between two consecutive pilot symbols, and there are N_p pilot symbols in a frame [32], [33]. Different symbols in each frame are denoted as $[x_1^p, x_{1,1}^d, \dots, x_{N_d,1}^d, x_2^p, x_{1,2}^d, \dots, x_{N_d,2}^d, \dots, x_{N_d,N_p-1}^d, x_{N_p}^p]$, where x_i^p denotes the i -th pilot symbol, and $[x_{1,i}^d, \dots, x_{N_d,i}^d]$ denotes data symbols between the i th and $(i+1)$ th pilot symbols.

A. Phase 1: Estimation of Interference and Channel Coefficients

In the first phase, we are interested in estimating \mathbf{c} and $\mathbf{h}_n^p, n = 1, \dots, N_p$ given the observations $\mathbf{y}_{1:N_p}^p$. For brevity, the superscript p is omitted in this section, i.e., x_i^p becomes x_i and we denote $\mathbf{Y} = [\mathbf{y}_{1:n-1}, \mathbf{y}_n, \mathbf{y}_{n+1:N_p}]$. Note that the EICs \mathbf{c} are unknown, deterministic parameters within a frame. As for \mathbf{h}_n , we have the knowledge of the distribution of \mathbf{h}_n , so

we use the MAP criteria to estimate \mathbf{h}_n . Therefore, the joint estimation criteria for \mathbf{c} and \mathbf{h}_n can be expressed as

$$\begin{aligned} \{\tilde{\mathbf{c}}_n, \tilde{\mathbf{h}}_n\} &= \operatorname{argmax}_{\mathbf{c}, \mathbf{h}_n} p(\mathbf{h}_n | \mathbf{Y}, \mathbf{c}) \\ &= \operatorname{argmax}_{\mathbf{c}, \mathbf{h}_n} p(\mathbf{h}_n, \mathbf{Y} | \mathbf{c}). \end{aligned} \quad (10)$$

For notational convenient, we omit \mathbf{c} in the following distributions, when there is no confusion, i.e., $p(\mathbf{h}_n | \mathbf{Y}, \mathbf{c})$ is simply written as $p(\mathbf{h}_n | \mathbf{Y})$. The prior distribution of \mathbf{h}_n is $p(\mathbf{h}_n) = \mathcal{CN}(\mathbf{h}_n, \mathbf{0}, \mathbf{I}_{N_r})$, where $\mathcal{CN}(\mathbf{x}, \boldsymbol{\mu}, \boldsymbol{\Sigma})$ is the complex Gaussian density of random vector \mathbf{x} having mean $\boldsymbol{\mu}$ and covariance matrix $\boldsymbol{\Sigma}$ [25]. Therefore, to estimate \mathbf{h}_n according to (10), we need to find $p(\mathbf{Y} | \mathbf{h}_n)$. This is because

$$p(\mathbf{h}_n, \mathbf{Y}) = p(\mathbf{Y} | \mathbf{h}_n) p(\mathbf{h}_n). \quad (11)$$

We provide the following theorem which states the log likelihood of received signals and channel coefficients at pilot positions.

Theorem 1. *The log likelihood of the received signals and channel coefficients at pilot position n is*

$$\begin{aligned} \mathcal{L}_{\mathbf{h}_n, \mathbf{Y}} &= \log(p(\mathbf{h}_n, \mathbf{Y})) \\ &= - \sum_{i=1}^{N_p} (\mathbf{y}_i - \boldsymbol{\mu}_{i,n})^H \boldsymbol{\Sigma}_{i,n}^{-1} (\mathbf{y}_i - \boldsymbol{\mu}_{i,n}) - \mathbf{h}_n^H \mathbf{h}_n + \text{const.} \end{aligned} \quad (12)$$

Proof. The proof and related parameters can be found in Appendix A. \square

We estimate the desired channel and EIC by maximizing $\mathcal{L}_{\mathbf{h}_n, \mathbf{Y}}$. As can be shown in the derivation later, the exponent of $p(\mathbf{h}_n, \mathbf{Y} | \mathbf{c})$ can be decomposed into two quadratic terms where one term contains \mathbf{h}_n and the other contains only \mathbf{c} and not \mathbf{h}_n . Since there are two variables to be optimized (i.e., \mathbf{h}_n and \mathbf{c}), we first derive the optimal \mathbf{h}_n with respect to \mathbf{c} then we derive the optimal \mathbf{c} by maximizing the corresponding objective function achieved with the optimal \mathbf{h}_n .

★ *Step 1: Derivation of the optimal \mathbf{h}_n for a given \mathbf{c}*

The sum of quadratic terms in (12) can be re-written as

$$\begin{aligned} \tilde{\mathcal{L}}_{\mathbf{h}_n, \mathbf{Y}} &= - \mathbf{h}_n^H \mathbf{h}_n \\ &\quad - \sum_{i=1}^{N_p} (\mathbf{y}_{i,n} - x_{i,n} \mathbf{h}_n - \mathbf{B}_{i,n} \mathbf{c})^H \boldsymbol{\Sigma}_{i,n}^{-1} (\mathbf{y}_{i,n} - x_{i,n} \mathbf{h}_n - \mathbf{B}_{i,n} \mathbf{c}) \\ &= - (\mathbf{h}_n - \tilde{\mathbf{h}}_n)^H \mathbf{A}_n (\mathbf{h}_n - \tilde{\mathbf{h}}_n) - \mathcal{C}_n, \end{aligned} \quad (13)$$

where we omit the constant in (12). $\mathbf{A}_n, \tilde{\mathbf{h}}_n$ and \mathcal{C}_n are defined below.

$$\begin{aligned}\mathbf{A}_n &= \mathbf{I}_{N_r} + \sum_{i=1}^{N_p} \omega_{i,n}^2 \boldsymbol{\Sigma}_{i,n}^{-1}, \\ \tilde{\mathbf{h}}_n &= \mathbf{A}_n^{-1} \left(\sum_{i=1}^{N_p} x_{i,n}^* \boldsymbol{\Sigma}_{i,n}^{-1} (\mathbf{y}_{i,n} - \mathbf{B}_{i,n} \mathbf{c}) \right), \\ \mathcal{C}_n &= -\tilde{\mathbf{h}}_n^H \mathbf{A}_n \mathbf{h}_n + \sum_{i=1}^{N_p} (\mathbf{y}_{i,n} - \mathbf{B}_{i,n} \mathbf{c})^H \boldsymbol{\Sigma}_{i,n}^{-1} (\mathbf{y}_{i,n} - \mathbf{B}_{i,n} \mathbf{c}),\end{aligned}\quad (14)$$

where $\omega_{i,n}, x_{i,n}, \mathbf{y}_{i,n}, \mathbf{B}_{i,n}$ and the related parameters are defined in (16)-(17). For notational simplicity, we denote the ‘sign indicator’ $j_{i,n} = -1$ for $i > n$, $j_{i,n} = 1$ for $i < n$ and $j_{i,n} = 0$ for $i = n$. Since \mathbf{A}_n is positive definite, the optimal \mathbf{h}_n that maximizes $\tilde{\mathcal{L}}_{\mathbf{h}_n, \mathbf{Y}}$ in (13) is $\tilde{\mathbf{h}}_n$. Note that, when desired channels are independent, we have $\mathbf{A}_n = a_n \mathbf{I}_{N_r}$, where

$$a_n = 1 + \sum_{i=1}^{N_p} \frac{\omega_{i,n}^2}{\sigma_{i,n}^2}. \quad (15)$$

★ *Step 2: Derivation of the optimal \mathbf{c}*

When $\mathbf{h}_n = \tilde{\mathbf{h}}_n$, the function in (13) is equal to $-\mathcal{C}_n$ which only depends on \mathbf{c} where

$$\begin{aligned}\mathcal{C}_n &= \sum_{i=1}^{N_p} (\mathbf{y}_{i,n} - \mathbf{B}_{i,n} \mathbf{c})^H \boldsymbol{\Sigma}_{i,n}^{-1} (\mathbf{y}_{i,n} - \mathbf{B}_{i,n} \mathbf{c}) \\ &\quad - \left\{ \left(\sum_{i=1}^{N_p} x_{i,n}^* \boldsymbol{\Sigma}_{i,n}^{-1} (\mathbf{y}_{i,n} - \mathbf{B}_{i,n} \mathbf{c}) \right)^H \mathbf{A}_n^{-1} \right. \\ &\quad \left. \left(\sum_{i=1}^{N_p} x_{i,n}^* \boldsymbol{\Sigma}_{i,n}^{-1} (\mathbf{y}_{i,n} - \mathbf{B}_{i,n} \mathbf{c}) \right) \right\} \\ &= (\mathbf{c} - \tilde{\mathbf{c}}_n)^H \mathbf{D}_n (\mathbf{c} - \tilde{\mathbf{c}}_n) + \text{const.},\end{aligned}\quad (22)$$

where \mathbf{D}_n and $\tilde{\mathbf{c}}_n$ are defined in (18),(19). It can be verified that \mathbf{D}_n is positive definite by using the *Cauchy-Schwarz* inequality. The proof of this property can be found in Appendix B. Therefore, the optimal \mathbf{c} that maximizes $\tilde{\mathcal{L}}_{\mathbf{h}_n, \mathbf{Y}}$ in (13) is $\tilde{\mathbf{c}}_n$. We take average over all $\tilde{\mathbf{c}}_n, n = 1, \dots, N_p$ to yield a reduced-variance estimate of \mathbf{c} . Consequently, the resulting estimated EIC vector can be written as

$$\tilde{\mathbf{c}} = \frac{1}{N_p} \sum_{n=1}^{N_p} \tilde{\mathbf{c}}_n. \quad (23)$$

The joint interference estimation, cancellation and channel estimation algorithm is described in Algorithm 1.

B. Symbol Detection

With the estimated $\tilde{\mathbf{c}}$, we can subtract the interference and channel coefficients at pilot positions are estimated as $\tilde{\mathbf{h}}_n$ given in (14) with \mathbf{c} substituted by $\tilde{\mathbf{c}}$ in (23). The estimated channel coefficients at pilot positions will be used for symbol detection in the following.

We will describe the symbol detection for the interval $x_i^p x_{1,i}^d x_{2,i}^d \dots x_{N_d,i}^d x_{i+1}^p$. The method can be applied and repeated for other intervals. For simplicity, we omit the pilot index i and superscript (d) in this section, i.e., the channel coefficients are denoted as $[\mathbf{h}_h, \mathbf{h}_{1:N_d}, \mathbf{h}_t]$, where \mathbf{h}_h represents the known channel coefficient at the pilot symbol right before

Algorithm 1 Estimation of EICs, Desired Channel Coefficients, and Interference Cancellation

- 1: **for** $n = 1 : N_p$ **do**
 - 2: **for** $i = 1 : N_p$ **do**
 - 3: Compute $x_{i,n}, \mathbf{y}_{i,n}, \mathbf{B}_{i,n}, \boldsymbol{\Sigma}_{i,n}$ in (14),(16).
 - 4: **end for**
 - 5: Compute $\mathbf{A}_n, \mathbf{D}_n$, and then $\tilde{\mathbf{c}}_n$ in (14), (18),(19).
 - 6: **end for**
 - 7: Compute $\tilde{\mathbf{c}}$ in (23) and subtract interference.
 - 8: **for** $n = 1 : N_p$ **do**
 - 9: Estimate \mathbf{h}_n as $\tilde{\mathbf{h}}_n$ in (14).
 - 10: **end for**
 - 11: End of algorithm.
-

the considered interval and \mathbf{h}_t represents known channel coefficient at the pilot symbol right after the considered interval.

In [34], the optimum diversity detection (called ODD for short) is derived to detect symbols individually based on interpolated channel coefficients at the corresponding positions if there is no interference (or the interference is canceled out). This method, however, requires expensive matrix inversion because the matrix size corresponds to the number of pilot symbols. Alternatively, we provide two different symbol detection methods where the first method is based on series symbol detection, which will be shown to outperform the optimum individual detector ODD at the expense of higher complexity, while the second method achieves very close (almost identical) SER to that due to ODD but with significantly lower complexity. These detection methods are described in the following.

1) *Series Symbol MAP Detection*: The symbols in an interval are detected as

$$\tilde{\mathbf{x}}_{1:N_d} = \arg \max_{\mathbf{x}} p(\mathbf{x}_{1:N_d} | \mathbf{h}_h, \mathbf{h}_t, \mathbf{y}_{1:N_d}). \quad (24)$$

We now characterize the log likelihood function in the following theorem.

Theorem 2. *The log likelihood of data symbols conditioned on received signals and channel coefficients at pilot positions right after and before the interval can be expressed in a sum of quadratic functions of data symbols \mathbf{x} as*

$$\log(p(\mathbf{x}_{1:N_d} | \mathbf{h}_h, \mathbf{h}_t, \mathbf{y}_{1:N_d})) = \mathcal{F} + \text{const.}, \quad (25)$$

where \mathcal{F} and related parameters can be found in (20, 21) and appendix F.

Proof. The proof and related parameters can be found in Appendix F. \square

By enumerating all possible vectors $\mathbf{x} = [x_1, \dots, x_{N_d}]$ from the constellation points and calculate the corresponding $p(\mathbf{x}_{1:N_d} | \mathbf{h}_h, \mathbf{h}_t, \mathbf{y}_{1:N_d})$, we are able to obtain the optimally detected symbols.

$$x_{i,n} = \omega_{i,n} x_i, \quad \mathbf{y}_{i,n} = \mathbf{y}_i - \beta_{i,n} \mathbf{y}_{i+j_{i,n}}, \quad \mathbf{B}_{i,n} = \mathbf{B}_i - \beta_{i,n} \mathbf{B}_{i+j_{i,n}}. \quad (16)$$

$$\omega_{i,n} = \begin{cases} \frac{\alpha_p^{n-i}}{1 + \rho(1 - \alpha_p^{2(n-i-1)})}, & i \neq n \\ 1, & i = n \end{cases}, \quad \beta_{i,n} = \begin{cases} \frac{x_i x_{i+j_{i,n}}^* \rho \alpha_p (\alpha_p^{2i-2n+2j_{i,n}-1})}{1 + j_{i,n} \rho (\alpha_p^{2i-2n+2j_{i,n}-1})}, & i \neq n \\ 0, & i = n \end{cases}. \quad (17)$$

$$\mathbf{D}_n = \sum_{i=1}^{N_p} \mathbf{B}_{i,n}^H \boldsymbol{\Sigma}_{i,n}^{-1} \mathbf{B}_{i,n} - \left(\sum_{i=1}^{N_p} x_{i,n}^* \boldsymbol{\Sigma}_{i,n}^{-1} \mathbf{B}_{i,n} \right)^H \mathbf{A}_n^{-1} \left(\sum_{i=1}^{N_p} x_{i,n}^* \boldsymbol{\Sigma}_{i,n}^{-1} \mathbf{B}_{i,n} \right). \quad (18)$$

$$\tilde{\mathbf{c}}_n = \mathbf{D}_n^{-1} \left\{ \sum_{i=1}^{N_p} \mathbf{B}_{i,n}^H \boldsymbol{\Sigma}_{i,n}^{-1} \mathbf{y}_{i,n} - \left(\sum_{i=1}^{N_p} x_{i,n}^* \boldsymbol{\Sigma}_{i,n}^{-1} \mathbf{B}_{i,n} \right)^H \mathbf{A}_n^{-1} \left(\sum_{i=1}^{N_p} x_{i,n}^* \boldsymbol{\Sigma}_{i,n}^{-1} \mathbf{y}_{i,n} \right) \right\}. \quad (19)$$

$$\mathcal{F} = \sum_{i=1}^{N_d} \left[\left(\tau_2 \boldsymbol{\Gamma}_{i,1} \mathbf{h}_h + \mathbf{1}_{i=N_d} \tau_2 \mathbf{h}_t + \sum_{j=1}^i \frac{x_j^*}{\sigma^2} \boldsymbol{\Gamma}_{i,j} \mathbf{y}_j \right)^H \mathbf{S}_i \left(\tau_2 \boldsymbol{\Gamma}_{i,1} \mathbf{h}_h + \mathbf{1}_{i=N_d} \tau_2 \mathbf{h}_t + \sum_{j=1}^i \frac{x_j^*}{\sigma^2} \boldsymbol{\Gamma}_{i,j} \mathbf{y}_j \right) \right]. \quad (20)$$

$$\mathbf{S}_i^{-1} = \left[\frac{1}{\sigma^2} + (1 + \alpha^2) \tau_1 \right] \mathbf{I}_{N_r} - \mathbf{1}_{i>1} \tau_2^2 \mathbf{S}_{i-1}, \quad \tilde{\mathbf{h}}_i = \begin{cases} \mathbf{S}_i \left[\tau_2 \boldsymbol{\Gamma}_{i,1} \mathbf{h}_h + \tau_2 \mathbf{h}_{i+1} + \sum_{j=1}^i \frac{x_j^*}{\sigma^2} \boldsymbol{\Gamma}_{i,j} \mathbf{y}_j \right], & i < N_d \\ \mathbf{S}_i \left[\tau_2 \boldsymbol{\Gamma}_{i,1} \mathbf{h}_h + \tau_2 \mathbf{h}_t + \sum_{j=1}^i \frac{x_j^*}{\sigma^2} \boldsymbol{\Gamma}_{i,j} \mathbf{y}_j \right], & i = N_d \end{cases}. \quad (21)$$

Algorithm 2 Symbol Detection Over Fast Fading Channel (I-MAP)

- 1: **for** $n = 1 : N_p$ **do**
 - 2: **for** $i = 1 : N_d$ **do**
 - 3: Estimate $\tilde{x}_{i,n}^d$ from (27) and assign $\tilde{x}_{i,n}^d$ to the closest point in the constellation.
 - 4: **end for**
 - 5: **end for**
 - 6: End of algorithm.
-

2) *Individual Symbol MAP Detection*: The symbol detection method presented in [26] determines the detected symbol x_i based on (24). However, because \tilde{x}_i is computed from $\tilde{x}_j, j < i$, this method suffers from error propagation, which increases the error rates of symbols in the middle of the interval. To address this limitation, we propose to estimate x_i individually as

$$\tilde{x}_i = \operatorname{argmax}_x p(x_i | \mathbf{h}_h, \mathbf{h}_t, \mathbf{y}_i). \quad (26)$$

Using similar derivations as those using to obtain the results in Theorem 2, we have²

$$\tilde{x}_i = \frac{\check{\mathbf{h}}_i^H \mathbf{y}_i}{\|\check{\mathbf{h}}_i\|^H}, \quad i = 1, \dots, N_d, \quad (27)$$

$$\check{\mathbf{h}}_i = \frac{\alpha^i}{1 - \alpha^{2i}} \mathbf{h}_h + \frac{\alpha^{N_d+1-i}}{1 - \alpha^{2(N_d+1-i)}} \mathbf{h}_t.$$

Then, detected symbols can be found by mapping \tilde{x}_i to the closest point in the constellation. This method does not suffer from error propagation and its achievable performance is less sensitive to positions of the data symbols in each detection interval. We summarize the proposed joint channel estimation and symbol detection in Algorithm 2.

²Upon deriving $\check{\mathbf{h}}_i$, the normalized technique employed is similar to that employed in the well-known Maximal Ratio Combining technique.

IV. PERFORMANCE ANALYSIS

In this section, we conduct performance analysis for the proposed design framework. For benchmarking, we first consider the interference-free scenario and inspect the effects of AWGN and channel evolutionary noise to the residual interference ν_n . As will be shown from the analysis, the power of channel estimation error (CEE) in the interference-free scenario approaches zero as the SNR tends to infinity. In the considered interference scenario, Furthermore, if the interfering channel power coefficients are identical, we prove that the residual interference and the channel estimation error are independent of the interfering power. Finally, based on the analysis of the estimation error, we demonstrate how the actual residual interference affects the symbol detection and derive the achievable SER.

In the following analysis, we investigate the channel estimation error (CEE, denoted as ν_n) and residual interference (denoted as \mathbf{v}_n) which are defined as follows:

$$\nu_n = \mathbf{h}_n - \tilde{\mathbf{h}}_n, \quad (28)$$

$$\mathbf{v}_n = \mathbf{B}_n (\mathbf{c} - \tilde{\mathbf{c}}).$$

A. Channel Estimation in Interference-free Scenario

In case of interference-free, the estimate of \mathbf{h}_n is

$$\tilde{\mathbf{h}}_n = \mathbf{A}_n^{-1} \left(\sum_{i=1}^N x_{i,n}^* \boldsymbol{\Sigma}_{i,n}^{-1} \mathbf{y}_{i,n} \right). \quad (29)$$

We characterize the performance of this channel estimator in the following proposition.³

Proposition 1. *The channel estimation error ν_n has Gaussian distribution with zero mean. Moreover, the effect of channel evolutionary noise to the channel estimation error is negligible as the SNR tends to infinity.*

³The fact that the effect of channel evolutionary noise diminishes as SNR goes to infinity suggests that the error floor in channel estimation reported in [26] comes from the residual interference. The analysis in the following will confirm this prediction.

Proof. Please see Appendix C. \square

B. Residual Interference Analysis

For the derived estimators for \mathbf{c} and \mathbf{h}_n under the considered interference scenario, the resulting residual interference is characterized in the following propositions.

Proposition 2. *The EIC estimation is unbiased and the residual interference follows the Gaussian distribution with zero mean. Moreover, the residual interference is independent of \mathbf{c} and has bounded power as the interference power goes to infinity.*

Proof. Please see Appendix D. \square

Proposition 3. *There is a floor for the residual interference power, i.e., as ρ goes to infinity, the residual interference power will approach $\tilde{\sigma}_i^2 = \frac{\alpha_p^2(1-\alpha_p^2)}{N_p}$.*

Proof. Please see Appendix E. \square

The channel estimation is performed based on the observations after interference cancellation. Therefore, a floor of residual interference will correspond to a floor in channel estimation performance. This also means that the achieved SINR after cancellation is bounded. This result is stated in the following proposition.

Proposition 4. *As the SNR goes to infinity, the SINR after interference cancellation⁴ approaches $\tilde{\rho} = \frac{N_p}{\alpha_p^2(1-\alpha_p^2)}$.*

Proof. After interference cancellation, the achievable SINR is affected by the channel estimation error and the residual interference. According to Proposition 1, the channel estimation error vanished as $\rho \rightarrow \infty$. Hence, the SINR after interference cancellation is $1/\tilde{\sigma}_i^2$, where $\tilde{\sigma}_i^2$ is given in Proposition 3. \square

C. SER Analysis

The unnormalized \tilde{x}_i is $\check{\mathbf{h}}_i^H (\mathbf{h}_i x_i + \tilde{\mathbf{w}}_i)$, where $\tilde{\mathbf{w}}_i$ is the sum of the additive Gaussian noise and residual interference with the corresponding covariance matrix of $(\sigma^2 + \sigma_i^2)\mathbf{I}_{N_r}$. Conditioned on \mathbf{h}_h and \mathbf{h}_t , the equivalent SNR for symbol detection of x_i can be expressed as

$$\rho_i^e = \frac{\alpha^{2i} \left\| \mathbf{h}_h \right\|^2 \frac{\alpha^i}{1-\alpha^{2i}} + \mathbf{h}_h^H \mathbf{h}_t \frac{\alpha^j}{1-\alpha^{2j}}}{(\sigma^2 + \sigma_i^2 + 1 - \alpha^{2i}) \left| \mathbf{h}_h^H \mathbf{1}_{N_r} \frac{\alpha^i}{1-\alpha^{2i}} + \mathbf{h}_t^H \mathbf{1}_{N_r} \frac{\alpha^j}{1-\alpha^{2j}} \right|^2}, \quad (30)$$

where $j = N_d + 1 - i$ and σ_i^2 can be computed from (48) or approximated by $\tilde{\sigma}_i^2$ in Proposition 3 for large ρ . Thus, the SER at symbol position i can be calculated as

$$P_i^e = \int p(\mathbf{h}_h, \mathbf{h}_t) f_e(\rho_i^e) d\mathbf{h}_h d\mathbf{h}_t, \quad (31)$$

⁴Since the interference is efficiently canceled, the probably most important parameter before interference cancellation is the SNR; therefore, we use the term "SNR before cancellation" but not "SINR before cancellation" to reflect this. After interference cancellation, the residual interference is irreducible and affects directly the performance of the detection process; hence, the term "SINR after cancellation" is used.

where $f_e(\rho)$ is the error rate corresponding to instantaneous ρ . For the QPSK modulation, $f_e(\rho) = \text{erfc}(\sqrt{\rho/2}) - \frac{1}{4} \text{erfc}^2(\sqrt{\rho/2})$, and $\text{erfc}(x) = \frac{2}{\sqrt{\pi}} \int_x^\infty e^{-x^2} dx$ is the complementary error function. The close-formed expression for P_i^e in (31) is difficult to derive. However, P_i^e can be computed accurately by using numerical integration or by Monte Carlo simulation. Finally, the overall average SER could be expressed as

$$P^e = \frac{1}{N_d} \sum_{i=1}^{N_d} P_i^e. \quad (32)$$

D. Throughput Analysis

The throughput is defined as the average number of successfully transmitted data symbol per symbol period, which is averaged over the frame interval. Note that there are N_d transmitted data symbols between two consecutive pilot symbols and the frame consists of N_p pilot symbols as shown in Fig. 1. Considering the average SER P^e in 32, the throughput can be calculated as

$$TP = (1 - P^e) \frac{N_d(N_p - 1)}{(N_d + 1)(N_p - 1) + 1}. \quad (33)$$

The pilot density is defined as $1/(N_d + 1)$. It can be verified that when we increase the pilot density (i.e., smaller N_d), P_e decreases; thus the first term in (33) increases. However, the increasing pilot density leads to higher pilot overhead which reduces the second term in (33) and vice versa. Thus, there is a trade-off between transmission reliability and throughput, which suggests that there exists an optimal value of the pilot density that achieves the maximum throughput.

Because the BER in (31) and the average SER in (32) cannot be expressed in closed form, the optimal pilot density for given α and ρ can be found effectively by using the bisection search method.

V. NUMERICAL RESULTS

We consider the simulation setting in which the desired receiver has $N_r = 2$ antennas, the coefficient α is chosen in the set $\{0.95, 0.99, 0.999\}$. The bandwidth of the interfering signal is two times of the bandwidth of the desired signal, which are 80kHz and 40kHz , respectively. The frequency spacing Δ_f between interfering and desired signals will be normalized as $\Delta_f T^d$ where T^d denotes the symbol time of the desired signal. We assume that the QPSK modulation is employed; both interfering and interfered signals use the root-raised-cosine pulse shaping function. Moreover, the pulse shaping functions $p^d(t)$ and $p^i(t)$ are assumed to have the roll-off factor equal to 0.25.

The interference power is set as strong as the power of the desired signal and the frequency spacing $\Delta_f = 1/T^d$ unless stated otherwise. The frame length is 201. When $N_d = 3$ (i.e., the pilot density is 25%), each frame consists of $N_p = 51$ pilot symbols and 150 data symbols; when $N_d = 4$ (i.e., the pilot density is 20%), each frame consists of $N_p = 41$ pilot symbols

and 160 data symbols. The results presented in this section are obtained by averaging over 10^4 random realizations.

For the interference-free scenario, we investigate the effect of different parameters to the channel estimation errors. The ideal case is the one where the channel coefficients are known perfectly, i.e., no fast fading and no channel estimation error. We will show the numerical mean square error for the channel estimation and residual interference power which are calculated as

$$\begin{aligned} \text{MSE}^h &= \frac{1}{N_p} \sum_{n=1}^{N_p} \mathbb{E} \left[(\mathbf{h}_n - \tilde{\mathbf{h}}_n) (\mathbf{h}_n - \tilde{\mathbf{h}}_n)^H \right], \\ \text{MSE}^i &= \frac{1}{N_r} \text{tr} \left(\mathbb{E}_{\mathbf{B}} \left[\mathbf{B} (\mathbf{c} - \tilde{\mathbf{c}}) (\mathbf{c} - \tilde{\mathbf{c}})^H \mathbf{B}^H \right] \right). \end{aligned} \quad (34)$$

In Fig. 2, we show the channel estimation error due to our proposed design for different values of α , when there is no interference (IF) and when there is interference (IP). For the interference-free scenario, the corresponding error curves converge to each other and decrease almost linearly as the SNR increases (both curves are plotted in the log scale). This means that the impact of the fast fading is diminished in the high SNR regime. When interference is present, there is a performance floor for channel estimation error. The results in Fig. 2 also validate the theoretical results stated in Propositions 1, 3, and 4 about the channel estimation errors in the scenarios without and with interference.

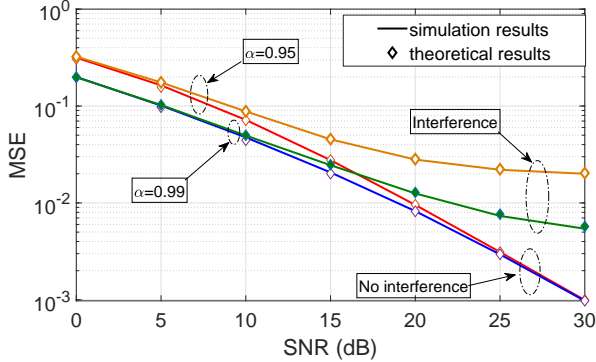


Fig. 2: Channel estimation MSE, $N_d = 3$

In Fig. 3, we show the residual interference power (RIP) and the squared channel estimation error (SCEE) versus SNR for different values of α . This figure confirms the performance floor whose value depends on α . More interestingly, the RIP and SCEE converge to almost the same value as the SNR increases. Note that we have assumed unity signal power, which explains the similar values of RIP and SCEE. This result suggests that the performance floor of desired channel estimation is caused by estimation errors of EICs.

In Fig. 4, we show the achieved SINR after interference cancellation versus the SNR for different values of channel correlation coefficient α . It can be seen that the achieved SINR increases with increasing SNR before becoming saturated. In the low SNR regime, however, the residual interference has almost no impact on the achieved SINR after interference cancellation, i.e., the SINR curves after interference cancellation

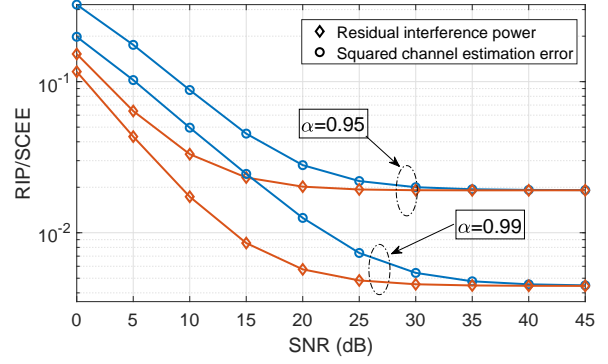


Fig. 3: Residual interference power and (RIP) and the squared channel estimation error (SCEE) versus SNR

are almost overlapped with the line showing the SNR before interference cancellation.

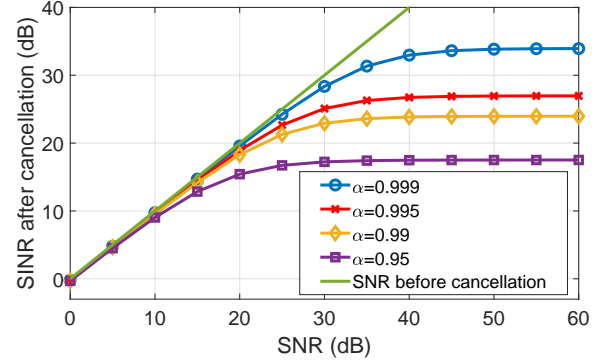


Fig. 4: SINR after cancellation for different values of channel correlation coefficient

We now compare the SER performance of series symbol MAP detection (S-MAP), individual symbol MAP detection (I-MAP) and optimum diversity detection (ODD) [23], [34] methods. Fig. 5 illustrates the SER achieved by these detection methods for interference-free and interfering scenarios. It can be seen that the SER of the proposed I-MAP is almost identical to that achieved by ODD. Moreover, the S-MAP detector outperforms both I-MAP and ODD and the performance gap is larger in the interference-free scenario. Note that, residual interference is still present which causes the error floor in these SER curves.

In Fig. 6, we show the SNR gap to achieve the same SER between different symbol detection methods (S-MAP, I-MAP) and scenarios (IF, IP). For the same scenario (IF or IP), the SNR gap between the proposed S-MAP and ODD becomes larger as the required SER decreases. Note again that there is a performance floor in the IP scenario, nevertheless, our proposed detection method achieves more than 3dB SNR gain compared to the existing ODD method for the same detection performance in the low target SER regime (see the curve with square markers). Moreover, to achieve the same SER performance under the high reliability condition (i.e., low SER), the SNR required in the interference scenario is much

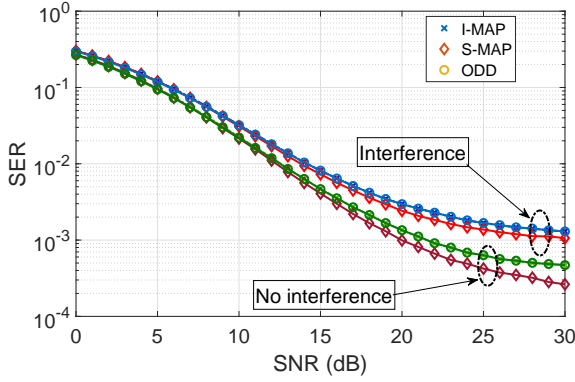


Fig. 5: SER achieved by different detection methods higher than that required in the interference free scenario.

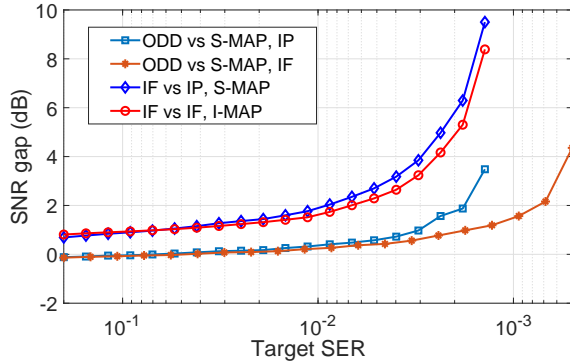


Fig. 6: SNR gap for specific target SER

Fig. 7 illustrates the SER in the interference-free and interference scenarios for different bandwidth ratios (denoted as BWR). As can be seen from the figure, higher bandwidth ratios between interference and desired signals cause higher SER. This is because higher BWR creates more severe interference for the desired signal and it is not possible to completely remove the interference due to the fast fading and channel correlation.

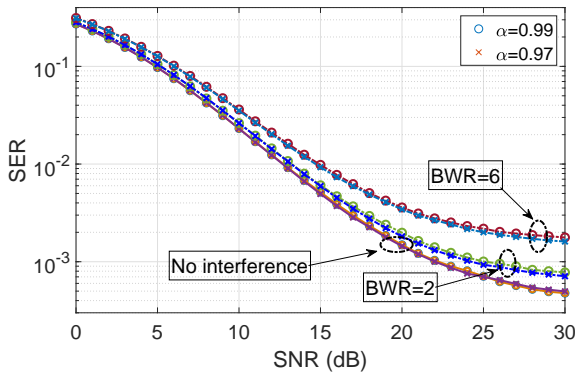


Fig. 7: SER versus SNR for different values of BWR

In Fig. 8, we show the variations of the throughput with the pilot density for different values of SNR ρ and channel correlation coefficient α . As can be seen from this figure, for given α and ρ , there exists an optimal pilot density that achieves the maximum throughput. Moreover, the maximum throughput increases as the SNR ρ increases. It can also be

observed that larger α leads to higher maximum throughput and lower optimal pilot density. This is because when the channel varies more slowly, the performance of interference cancellation and channel estimation is improved, which results in more reliable transmission and higher throughput. The results in this figure demonstrate the tradeoff between the throughput and communication reliability in the fast fading environment.

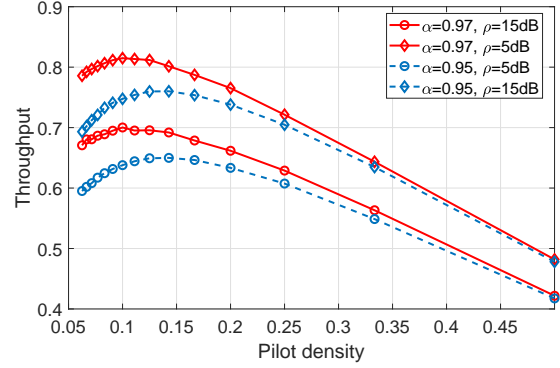


Fig. 8: Throughput variations with the pilot density

VI. CONCLUSION

We have proposed a two-phase framework for channel estimation, interference cancellation, and symbol detection for communication signals with different bandwidth in the fast fading environment. Specifically, we have derived the channel estimators and studied both series and individual symbol detection methods. Numerical studies have confirmed the existence of the performance floor for SER in the considered interference scenario and illustrated the optimal pilot density to achieve the maximum throughput. Moreover, the numerical results have shown that the series symbol detection method outperforms the existing ODD method in term of SER while the individual symbol detection method achieves the very close performance to the ODD method but with lower complexity.

APPENDIX A PROOF OF THEOREM 1

The likelihood of \mathbf{Y} , given \mathbf{h}_n can be factorized, thanks to the channel Markovian property, as

$$p(\mathbf{Y}|\mathbf{h}_n) = p(\mathbf{y}_n|\mathbf{h}_n) \prod_{i=1}^{n-1} p(\mathbf{y}_i|\mathbf{y}_{i+1}, \mathbf{h}_n) \prod_{i=n+1}^{N_p} p(\mathbf{y}_i|\mathbf{y}_{i-1}, \mathbf{h}_n). \quad (35)$$

Given \mathbf{h}_n , any two consecutive observations are correlated due to the cumulative channel evolutionary noises. Since we consider only received signals at pilot positions, the equivalent channel correlation coefficient is $\alpha_p = \alpha^{N_d+1}$. To further derive $p(\mathbf{Y}|\mathbf{h}_n)$, we need to find the probabilities $p(\mathbf{y}_i|\mathbf{y}_{i-1}, \mathbf{h}_n)$ for $i > n$ and $p(\mathbf{y}_i|\mathbf{y}_{i+1}, \mathbf{h}_n)$ for $i < n$. We first consider $p(\mathbf{y}_i|\mathbf{y}_{i-1}, \mathbf{h}_n)$ for $i > n$. Toward this end, we derive the joint

probability $p(\mathbf{y}_i, \mathbf{y}_{i-1} | \mathbf{h}_n)$. From (8), the channel coefficient $\mathbf{h}_i, i > n$ can be expressed with respect to \mathbf{h}_n as

$$\mathbf{h}_i = \alpha_p^{i-n} \left(\mathbf{h}_n + \eta_p \sum_{j=1}^{i-n} \alpha_p^{-j} \Delta_{n+j} \right), \quad (36)$$

where $\eta_p = (1 - \alpha_p^2)^{1/2}$. Substituting \mathbf{h}_n in (36) into (9), it can be seen that \mathbf{y}_i and \mathbf{y}_{i-1} share the common evolutionary noise terms $\Delta_{n+j}, j = 1, \dots, i-n-1$. Then, we can obtain the parameters of the distribution $p(\mathbf{y}_i, \mathbf{y}_{i-1} | \mathbf{h}_n) = \mathcal{CN} \left(\begin{bmatrix} \mathbf{y}_i \\ \mathbf{y}_{i-1} \end{bmatrix}, \begin{bmatrix} \boldsymbol{\mu}_{\mathbf{y}_i | \mathbf{h}_n} \\ \boldsymbol{\mu}_{\mathbf{y}_{i-1} | \mathbf{h}_n} \end{bmatrix}, \begin{bmatrix} \boldsymbol{\Sigma}_{\mathbf{y}_i | \mathbf{h}_n} & \boldsymbol{\Sigma}_{\mathbf{y}_i, \mathbf{y}_{i-1} | \mathbf{h}_n} \\ \boldsymbol{\Sigma}_{\mathbf{y}_i, \mathbf{y}_{i-1} | \mathbf{h}_n}^H & \boldsymbol{\Sigma}_{\mathbf{y}_{i-1} | \mathbf{h}_n} \end{bmatrix} \right)$ as follows:

$$\begin{aligned} \boldsymbol{\mu}_{\mathbf{y}_k | \mathbf{h}_n} &= \mathbf{B}_k \mathbf{c} + \alpha_p^{k-n} \mathbf{h}_n x_k, \quad k = i, i-1, \\ \boldsymbol{\Sigma}_{\mathbf{y}_k | \mathbf{h}_n} &= \left(\sigma^2 + \alpha_p^{2(k-n)} \eta_p^2 \sum_{j=1}^{k-n} \alpha_p^{-2j} \right) \mathbf{I}_{N_r}, \\ &= [1 + \rho (1 - \alpha_p^{2(k-n)})] \sigma^2 \mathbf{I}_{N_r}, \quad k = i, i-1, \quad (37) \\ \boldsymbol{\Sigma}_{\mathbf{y}_i, \mathbf{y}_{i-1} | \mathbf{h}_n} &= \mathbb{E} \left[\left(\mathbf{y}_i - \boldsymbol{\mu}_{\mathbf{y}_i | \mathbf{h}_n} \right) \left(\mathbf{y}_{i-1} - \boldsymbol{\mu}_{\mathbf{y}_{i-1} | \mathbf{h}_n} \right)^H \middle| \mathbf{h}_n \right] \\ &= x_i x_{i-1}^* \alpha_p (1 - \alpha_p^{2(i-n-1)}) \mathbf{I}_{N_r}. \end{aligned}$$

Next, we apply the conditional probability formula for the multivariate Complex Circular Symmetric Gaussian vector [35] (section 3.7.7, page 153) and obtain $p(\mathbf{y}_i | \mathbf{y}_{i-1}, \mathbf{h}_n) = \mathcal{CN}(\mathbf{y}_i, \boldsymbol{\mu}_{i,n}, \boldsymbol{\Sigma}_{i,n})$ for $i > n$, where

$$\begin{aligned} \boldsymbol{\mu}_{i,n} &= \boldsymbol{\mu}_{\mathbf{y}_i | \mathbf{h}_n} + \beta_{i,n} (\mathbf{y}_{i-1} - \boldsymbol{\mu}_{\mathbf{y}_{i-1} | \mathbf{h}_n}), \\ \boldsymbol{\Sigma}_{i,n} &= \sigma_{i,n}^2 \mathbf{I}_{N_r}, \quad \beta_{i,n} = \frac{x_i x_{i-1}^* \rho \alpha_p (1 - \alpha_p^{2(i-n-1)})}{1 + \rho (1 - \alpha_p^{2(i-n-1)})}, \quad (38) \\ \sigma_{i,n}^2 &= \sigma^2 \left[1 + \rho (1 - \alpha_p^{2(i-n)}) - \frac{\rho^2 \alpha_p^2 (1 - \alpha_p^{2(i-n-1)})^2}{1 + \rho (1 - \alpha_p^{2(i-n-1)})} \right]. \end{aligned}$$

For $i < n$, $p(\mathbf{y}_i | \mathbf{y}_{i+1}, \mathbf{h}_n) = \mathcal{CN}(\mathbf{y}_i, \boldsymbol{\mu}_{i,n}, \boldsymbol{\Sigma}_{i,n})$, where the parameters can be expressed similarly:

$$\begin{aligned} \boldsymbol{\mu}_{i,n} &= \alpha_p^{n-i} \mathbf{h}_n x_i + \mathbf{B}_i \mathbf{c} + \beta_{i,n} (\mathbf{y}_{i+1} - \alpha_p^{n-i-1} \mathbf{h}_n x_{i+1} - \mathbf{B}_{i+1} \mathbf{c}), \\ \boldsymbol{\Sigma}_{i,n} &= \sigma_{i,n}^2 \mathbf{I}_{N_r}, \quad \beta_{i,n} = \frac{x_i x_{i+1}^* \rho \alpha_p (1 - \alpha_p^{2(n-i-1)})}{1 + \rho (1 - \alpha_p^{2(n-i-1)})}, \quad (39) \\ \sigma_{i,n}^2 &= \sigma^2 \left[1 + \rho (1 - \alpha_p^{2(n-i)}) - \frac{\rho^2 \alpha_p^2 (1 - \alpha_p^{2(n-i-1)})^2}{1 + \rho (1 - \alpha_p^{2(n-i-1)})} \right]. \end{aligned}$$

For $j = n$, $\boldsymbol{\mu}_{n,n} = \mathbf{h}_n x_n + \mathbf{B}_n \mathbf{c}$, $\boldsymbol{\Sigma}_{n,n} = \sigma^2 \mathbf{I}_{N_r}$. Substituting the parameters in (38) and (39) into (11) using (35), taking the logarithm, we obtain the log-likelihood function in Theorem 1. This completes the proof.

APPENDIX B

PROOF FOR THE POSITIVE-DEFINITENESS OF \mathbf{D}_n

For an arbitrary non-zero vector $\mathbf{z} = [z_1, \dots, z_L]^T$, we have

$$\begin{aligned} \mathbf{z}^H \mathbf{D}_n \mathbf{z} &= \text{tr} \left[\left(\sum_{i=1}^{N_p} \frac{(\mathbf{B}_{i,n} \mathbf{z})^H (\mathbf{B}_{i,n} \mathbf{z})}{\sigma_{i,n}^2} \right) \right] \\ &= \text{tr} \left[\left(\sum_{i=1}^{N_p} \frac{x_{i,n}^* \mathbf{B}_{i,n} \mathbf{z}}{\sigma_{i,n}^2} \right)^H \mathbf{A}_n^{-1} \left(\sum_{i=1}^{N_p} \frac{x_{i,n}^* \mathbf{B}_{i,n} \mathbf{z}}{\sigma_{i,n}^2} \right) \right] \\ &= \text{tr} \left[\left(\sum_{i=1}^{N_p} \frac{(\mathbf{B}_{i,n} \mathbf{z}) (\mathbf{B}_{i,n} \mathbf{z})^H}{\sigma_{i,n}^2} \right) \right] \\ &= \text{tr} \left[\left(\sum_{i=1}^{N_p} \frac{x_{i,n}^* \mathbf{B}_{i,n} \mathbf{z}}{\sigma_{i,n}^2} \right)^H \mathbf{A}_n^{-1} \left(\sum_{i=1}^{N_p} \frac{x_{i,n}^* \mathbf{B}_{i,n} \mathbf{z}}{\sigma_{i,n}^2} \right) \right] \\ &> \text{tr} \left[\left(\sum_{i=1}^{N_p} \frac{(\mathbf{B}_{i,n} \mathbf{z}) (\mathbf{B}_{i,n} \mathbf{z})^H}{\sigma_{i,n}^2} \right) \right] \\ &= \left(\sum_{i=1}^{N_p} \frac{x_{i,n}^* \mathbf{B}_{i,n} \mathbf{z}}{\sigma_{i,n}^2} \right) (\mathbf{A}_n - \mathbf{I}_{N_r})^{-1} \left(\sum_{i=1}^{N_p} \frac{x_{i,n}^* \mathbf{B}_{i,n} \mathbf{z}}{\sigma_{i,n}^2} \right)^H, \quad (40) \end{aligned}$$

where $\text{tr}(\mathbf{X})$ is the sum of diagonal elements of \mathbf{X} . On the last two lines of (40), the j -th diagonal element of the first term is $\sum_{i=1}^{N_p} (\mathbf{b}_{i,n}^{(j)} \mathbf{z}) (\mathbf{b}_{i,n}^{(j)} \mathbf{z})^H / \sigma_{i,n}^2$, where $\mathbf{b}_{i,n}^{(j)}$ is the j -th row of $\mathbf{B}_{i,n}$, and the j -th diagonal element of the second term is $\left(\sum_{i=1}^{N_p} \frac{|x_{i,n}|^2}{\sigma_{i,n}^2} \right)^{-1} \left(\sum_{i=1}^{N_p} \frac{x_{i,n}^* \mathbf{b}_{i,n}^{(j)} \mathbf{z}}{\sigma_{i,n}^2} \right) \left(\sum_{i=1}^{N_p} \frac{x_{i,n} \mathbf{b}_{i,n}^{(j)} \mathbf{z}^H}{\sigma_{i,n}^2} \right)^H$, where \mathbf{A}_n from (14) is substituted into this term.

We now define the two vectors \mathbf{u} and \mathbf{v} whose i th elements are $u_i = x_{i,n}^* / \sigma_{i,n}$, $v_i = \mathbf{b}_{i,n}^{(j)} \mathbf{z} / \sigma_{i,n}$, respectively. By applying the *Cauchy-Schwarz* inequality

$$|\mathbf{u}|^2 |\mathbf{v}|^2 \geq |\mathbf{u} \cdot \mathbf{v}|^2, \quad (41)$$

it can be verified that each diagonal element of the matrix on the last two lines of (40) is positive, which means its trace is also positive. Thus, we have completed the proof.

APPENDIX C

PROOF OF PROPOSITION 1

The channel estimation error can be written as

$$\begin{aligned} \boldsymbol{\nu}_n &= \mathbf{h}_n - \mathbf{A}_n^{-1} \left(\sum_{i=1}^{N_p} \frac{x_{i,n}^*}{\sigma_{i,n}^2} (\mathbf{y}_i - \beta_{i,n} \mathbf{y}_{i+j_{i,n}}) \right) \\ &= \boldsymbol{\nu}_n^g + \boldsymbol{\nu}_n^c, \quad (42) \end{aligned}$$

Where $\boldsymbol{\nu}_n^g$ is the error due to the AWGN, and $\boldsymbol{\nu}_n^c$ is the error due to the channel evolutionary noise. Specifically,

$$\begin{aligned} \boldsymbol{\nu}_n^g &= \sum_{i=1}^{N_p} \Xi_{i,n}^g \mathbf{w}_i, \\ \boldsymbol{\nu}_n^c &= \Xi_{0,n}^c \mathbf{h}_0 + \sum_{i=1}^{N_p} \Xi_{i,n}^c \Delta_i, \quad (43) \end{aligned}$$

where we decompose \mathbf{h}_n into $\alpha_p^n (\mathbf{h}_0 + \sum_{i=1}^n \alpha_p^{-i} \Delta_i)$. By using this decomposition, it is more convenient to compute the channel estimation error components due to the channel evolutionary noise. Otherwise, one has to determine the dependence structure of \mathbf{h}_n on the preceding channel noise components $\Delta_i, i < n$, which is not trivial.

When the desired channels are independent, $\Xi_{i,n}^g = \xi_{i,n}^g \mathbf{I}_{N_r}$ and $\Xi_{i,n}^c = \xi_{i,n}^c \mathbf{I}_{N_r}$. Substituting $\mathbf{y}_i = \mathbf{h}_i x_i + \mathbf{w}_i$ into (42), we have

$$\xi_{i,n}^g = \begin{cases} -\frac{x_{i,n}^*}{a_n \sigma_{i,n}^2}, & i=1, n, n \pm 1, N_p, \\ -\frac{x_i^*}{a_n} \left(\frac{\omega_{i,n}}{\sigma_{i,n}^2} + \frac{|\beta_{n,i-j_i,n}| \omega_{n,i-j_i,n}}{\sigma_{n,i-j_i,n}^2} \right), & \text{otherwise.} \end{cases}$$

Hence, the AWGN contributes to the CEE with the total power of $\sigma^2 \sum_{i=1}^{N_p} |\xi_{i,n}^g|^2$. As the SNR goes to infinity, $\lim_{\rho \rightarrow \infty} \sum_{i=1}^{N_p} |\xi_{i,n}^g|^2 = 1$, and the AWGN contributes σ^2 to the overall CEE. Besides, ν_n^c is expressed in (45), and we can write the multipliers $\xi_{i,n}^c$ as follows:

$$\begin{aligned} \xi_{0,n}^c &= \alpha_p^n - \sum_{i=1}^{N_p} \frac{\omega_{i,n} \alpha_p^i}{a_n \sigma_{i,n}^2} (1 - |\beta_{i,n}| \alpha_p^{j_{i,n}}), \\ \xi_{i,n}^c &= \frac{\alpha_p^{-i}}{a_n} \left(\sum_{k=i-1}^{n-1} \frac{\omega_{k,n}}{\sigma_{k,n}^2} |\beta_{k,n}| \alpha_p^{k+1} - \sum_{k=i}^{N_p} \frac{\omega_{k,n}}{\sigma_{k,n}^2} \alpha_p^k \right. \\ &\quad \left. + \alpha_p^n + \sum_{k=n+1}^{N_p} \frac{\omega_{k,n}}{\sigma_{k,n}^2} |\beta_{k,n}| \alpha_p^{k-1} \right), \quad i \leq n, \\ \xi_{i,n}^c &= \frac{\alpha_p^{-i}}{a_n} \left(\sum_{k=i+1}^{N_p} \frac{\omega_{k,n}}{\sigma_{k,n}^2} |\beta_{k,n}| \alpha_p^{k-1} - \sum_{k=i}^{N_p} \frac{\omega_{k,n}}{\sigma_{k,n}^2} \alpha_p^k \right. \\ &\quad \left. - \frac{1}{\sigma^2} \mathbb{1}_{n < N} \mathbb{1}_{i=N} \right), \quad i > n. \end{aligned} \quad (44)$$

As SNR goes to infinity, $\lim_{\rho \rightarrow \infty} \sum_{i=1}^{N_p} |\xi_{i,n}^c|^2 = 0$, the channel evolutionary noises contribute negligible power to the CEE. This completes the proof.

APPENDIX D PROOF OF PROPOSITION 2

Substituting $\mathbf{y}_{i,n}$ from (16) into (19), note that $\mathbf{y}_i = \mathbf{h}_i x_i + \mathbf{B}_i \mathbf{c} + \mathbf{w}_i$, and after some manipulations, we have

$$\tilde{\mathbf{c}}_n = \mathbf{c} + \mathbf{D}_n^{-1} \sum_{i=1}^{N_p} \mathbf{G}_{i,n} (\mathbf{h}_i x_i + \mathbf{w}_i), \quad (46)$$

where $\mathbf{K}_n = \left(\sum_{i=1}^{N_p} x_{i,n}^* \Sigma_{i,n}^{-1} \mathbf{B}_{i,n} \right)^H \mathbf{A}_n^{-1}$, $\mathbf{J}_{i,n} = (\mathbf{B}_{i,n}^H - \mathbf{K}_n x_{i,n}^*) \Sigma_{i,n}^{-1}$, and

$$\mathbf{G}_{i,n} = \begin{cases} \mathbf{J}_{i,n}, & i=1, n, N_p \\ \mathbf{J}_{i,n} - \mathbf{J}_{i-1,n} \beta_{i-1,n}, & n > i > 1 \\ \mathbf{J}_{i,n} - \mathbf{J}_{i+1,n} \beta_{i+1,n}, & n < i < N_p. \end{cases} \quad (47)$$

The second term in (46) represents the estimation error of \mathbf{c} at position n , and it is independent of \mathbf{c} . This completes the proof for the first part of the proposition.

Additionally, it can be seen that the estimation error is a linear combination of zero-mean Gaussian random variables, hence it also has zero mean. Therefore, the estimation is unbiased. The covariance matrix of the residual interference at position n -th is

$$\begin{aligned} &(\sigma_h^2 + \sigma^2) \mathbb{E}_{(\mathbf{x}, \mathbf{B})} \left[\mathbf{B}_n \mathbf{D}_n^{-1} \left(\sum_{i=1}^{N_p} \mathbf{G}_{i,n} \mathbf{G}_{i,n}^H \right) \mathbf{D}_n^{-1} \mathbf{B}_n^H \right] + \\ &\sigma_h^2 \sum_{i \neq j} \mathbb{E}_{(\mathbf{x}, \mathbf{B}, \mathbf{h}_i, \mathbf{h}_j)} \left[\mathbf{B}_n \mathbf{D}_n^{-1} \left(\mathbf{G}_{i,n} \mathbf{h}_i \mathbf{h}_j^H \mathbf{G}_{j,n}^H x_i x_j^* \right) \mathbf{D}_n^{-1} \mathbf{B}_n^H \right] \\ &= (\sigma_h^2 + \sigma^2) \mathbb{E}_{(\mathbf{x}, \mathbf{B})} \left[\mathbf{B}_n \mathbf{D}_n^{-1} \left(\sum_{i=1}^{N_p} \mathbf{G}_{i,n} \mathbf{G}_{i,n}^H \right) \mathbf{D}_n^{-1} \mathbf{B}_n^H \right] + \\ &\sigma_h^2 \sum_{i \neq j} \alpha_p^{|i-j|} \mathbb{E}_{(\mathbf{x}, \mathbf{B})} \left[\mathbf{B}_n \mathbf{D}_n^{-1} \left(\mathbf{G}_{i,n} \mathbf{G}_{j,n}^H x_i x_j^* \right) \mathbf{D}_n^{-1} \mathbf{B}_n^H \right]. \end{aligned} \quad (48)$$

Deriving the closed-form expression for the covariance matrix is tedious. Hence, we will prove Proposition 2 by using the following arguments. First, note that, \mathbf{D}_n is Hermitian, positive definite, and in quadratic order of interfering matrices $\mathbf{B}_i, i = 1, \dots, N$. Second, $\mathbf{B}_n \mathbf{G}_{i,n}$ is also in quadratic order of interfering matrices. Therefore, the expected covariance matrix is in a fractional function form with total zero-th order of \mathbf{B}_i . As a result, the residual interference power is bounded as we increase the interference power to infinity. Furthermore, if all interfering channel coefficients for different antennas have identical value, the residual interference power is *completely* independent of the interference power. Since estimation errors for EICs at any symbol position n are finite, the overall estimation error for EICs is also finite. This completes the proof.

APPENDIX E PROOF OF PROPOSITION 3

Since the expression of the power of residual interference in (48) contains σ_h^2 , it does not vanish as $\rho \rightarrow \infty$. As ρ goes to infinity, we have

$$\begin{aligned}
\boldsymbol{\nu}_n^c &= \mathbf{h}_n - \mathbf{A}_n^{-1} \left\{ \sum_{i=1}^{N_p} \frac{\omega_{i,n} \alpha_p^i}{\sigma_{i,n}^2} \left[\mathbf{h}_0 + \sum_{k=1}^i \alpha_p^{-k} \boldsymbol{\Delta}_k - |\beta_{i,n}| \alpha_p^{j_{i,n}} \left(\mathbf{h}_0 + \sum_{k=1}^{i+j_{i,n}} \alpha_p^{-k} \boldsymbol{\Delta}_k \right) \right] \right\} \\
&= \mathbf{h}_0 \left(\alpha_p^n - \sum_{i=1}^{N_p} \frac{\omega_{i,n} \alpha_p^i}{a_n \sigma_{i,n}^2} (1 - |\beta_{i,n}| \alpha_p^{j_{i,n}}) \right) - \sum_{k=1}^{N_p} \left(\boldsymbol{\Delta}_k \alpha_p^{-k} \sum_{i=k}^{N_p} \frac{\omega_{i,n} \alpha_p^i}{a_n \sigma_{i,n}^2} \right) + \sum_{i=1}^n \alpha_p^{n-i} \boldsymbol{\Delta}_i \\
&+ \sum_{k=1}^n \left(\boldsymbol{\Delta}_k \alpha_p^{-k} \sum_{i=k-1}^{n-1} \frac{\omega_{i,n}}{a_n \sigma_{i,n}^2} |\beta_{i,n}| \alpha_p^{i+1} \right) + \sum_{k=1}^{N_p-1} \left(\boldsymbol{\Delta}_k \alpha_p^{-k} \sum_{i=k+1, i>n}^{N_p} \frac{\omega_{i,n}}{a_n \sigma_{i,n}^2} |\beta_{i,n}| \alpha_p^{i-1} \right) \\
&= \mathbf{h}_0 \left(\alpha_p^n - \sum_{i=1}^{N_p} \frac{\omega_{i,n} \alpha_p^i}{a_n \sigma_{i,n}^2} (1 - |\beta_{i,n}| \alpha_p^{j_{i,n}}) \right) + \sum_{k=n+1}^{N-1} \left[\boldsymbol{\Delta}_k \frac{\alpha_p^{-k}}{a_n} \left(\sum_{i=k+1}^{N_p} \frac{\omega_{i,n}}{\sigma_{i,n}^2} |\beta_{i,n}| \alpha_p^{i-1} - \sum_{i=k}^{N_p} \frac{\omega_{i,n}}{\sigma_{i,n}^2} \alpha_p^i \right) \right] \\
&+ \sum_{k=1}^n \left[\boldsymbol{\Delta}_k \frac{\alpha_p^{-k}}{a_n} \left(\sum_{i=k-1}^{n-1} \frac{\omega_{i,n}}{\sigma_{i,n}^2} |\beta_{i,n}| \alpha_p^{i+1} - \sum_{i=k}^{N_p} \frac{\omega_{i,n}}{\sigma_{i,n}^2} \alpha_p^i + \sum_{i=n+1}^{N_p} \frac{\omega_{i,n}}{\sigma_{i,n}^2} |\beta_{i,n}| \alpha_p^{i-1} \right) \right] + \sum_{k=1}^n \boldsymbol{\Delta}_k \alpha_p^{n-k} - \boldsymbol{\Delta}_N \frac{\omega_{N,n}}{a_n \sigma_{N,n}^2} \mathbf{1}_{n < N}.
\end{aligned} \tag{45}$$

APPENDIX F
PROOF OF THEOREM 2

We can reformulate $p(x_{1:N_d} | \mathbf{h}_h, \mathbf{h}_t, \mathbf{y}_{1:N_d})$ as follows:

$$\omega_{i,n} \rightarrow \begin{cases} \alpha_p, & i = n \pm 1 \\ 1, & i = n \\ 0, & \text{otherwise} \end{cases}, \quad |\beta_{i,n}| \rightarrow \begin{cases} 0, & i = n, n \pm 1 \\ \alpha_p, & \text{otherwise} \end{cases},$$

$$\sigma_{i,n}^2 \rightarrow \begin{cases} \sigma^2, & i = n \\ 1 - \alpha_p^2, & \text{otherwise} \end{cases},$$

$$\mathbf{A}_n \rightarrow \rho \mathbf{I}_{N_r},$$

$$\begin{aligned}
\mathbf{D}_n &\rightarrow \mathbf{B}_n^H \mathbf{B}_n + \sum_{i \neq n} \frac{\mathbf{B}_{i,n}^H \mathbf{B}_{i,n}}{1 - \alpha_p^2} + 2 \frac{\alpha_p^2}{1 - \alpha_p^2} \mathbf{B}_n^H \mathbf{B}_n \\
&- \frac{\alpha_p}{1 - \alpha_p^2} \sum_{i=n \pm 1} (x_i^* x_n \mathbf{B}_n^H \mathbf{B}_i + x_i x_n^* \mathbf{B}_i^H \mathbf{B}_n)
\end{aligned}$$

$$\rightarrow N_r N_p \frac{1 + \alpha_p^2}{1 - \alpha_p^2} \mathbf{I}_L,$$

$$\mathbf{K}_n \rightarrow x_n \mathbf{B}_n^H,$$

$$\mathbf{J}_{n,n} \rightarrow \mathbf{B}_n^H \frac{1 + \alpha_p^2}{1 - \alpha_p^2} - \frac{x_n^* \alpha_p}{1 - \alpha_p^2} \sum_{i=n \pm 1} x_i \mathbf{B}_i^H,$$

$$\mathbf{J}_{i,n} \rightarrow \frac{\mathbf{B}_{i,n}^H - x_n x_i^* \alpha_p \mathbf{B}_n^H}{1 - \alpha_p^2}, \quad i \neq n,$$

$$\begin{aligned}
\mathbf{J}_{i,n} \mathbf{J}_{i,n}^H &\rightarrow N_r \left(\frac{1 + |\beta_{i,n}|^2 + \omega_{i,n}^2}{\sigma_{i,n}^4} \right) \mathbf{I}_L \\
&\rightarrow \frac{N_r (1 + \alpha_p^2)}{(1 - \alpha_p^2)^2} \mathbf{I}_L, \quad i \neq n,
\end{aligned}$$

$$\begin{aligned}
\mathbf{G}_{i,n} \mathbf{G}_{i,n}^H &\rightarrow \mathbf{J}_{i,n} \mathbf{J}_{i,n}^H + |\beta_{i \pm 1, n}|^2 \mathbf{J}_{i \pm 1, n} \mathbf{J}_{i \pm 1, n}^H + \frac{2 N_r |\beta_{i \pm 1, n}|^2}{\sigma_{i,n}^2 \sigma_{i \pm 1, n}^2} \mathbf{I}_L \\
&\rightarrow N_r \frac{1 + \alpha_p^4 + 4 \alpha_p^2}{(1 - \alpha_p^2)^2} \mathbf{I}_L, \quad i \neq n.
\end{aligned} \tag{49}$$

Upon having these asymptotic values, we substitute these values into (48) to arrive at the residual interference power limit stated in the proposition. This completes the proof.

$$\begin{aligned}
p(x_{1:N_d} | \mathbf{h}_h, \mathbf{h}_t, \mathbf{y}_{1:N_d}) &\propto \int p(x_{1:N_d}, \mathbf{y}_{1:N_d}, \mathbf{h}_h, \mathbf{h}_{1:N_d}, \mathbf{h}_t) d\mathbf{h}_{1:N_d} \\
&\stackrel{(a)}{\propto} \int p(\mathbf{y}_{1:N_d} | \mathbf{h}_{1:N_d}, x_{1:N_d}) p(\mathbf{h}_h, \mathbf{h}_{1:N_d}, \mathbf{h}_t) d\mathbf{h}_{1:N_d} \\
&\stackrel{(b)}{\propto} \int p(\mathbf{h}_h, \mathbf{h}_{1:N_d}, \mathbf{h}_t) \prod_{i=1}^{N_d} p(\mathbf{y}_i | x_i, \mathbf{h}_i) d\mathbf{h}_{1:N_d} \\
&\stackrel{(c)}{\propto} \int p(\mathbf{h}_1 | \mathbf{h}_h) p(\mathbf{h}_t | \mathbf{h}_{N_d}) \prod_{i=2}^{N_d} p(\mathbf{h}_i | \mathbf{h}_{i-1}) \prod_{i=1}^{N_d} p(\mathbf{y}_i | x_i, \mathbf{h}_i) d\mathbf{h}_{1:N_d} \\
&\stackrel{(d)}{\propto} e^{\mathcal{F}} \int \exp \left\{ - \sum_{i=1}^{N_d} (\mathbf{h}_i - \mathbf{a}_i)^H \mathbf{S}_i^{-1} (\mathbf{h}_i - \mathbf{a}_i) \right\} d\mathbf{h}_{1:N_d} \\
&\stackrel{(e)}{\propto} e^{\mathcal{F}} \prod_{i=1}^{N_d} |\mathbf{S}_i|,
\end{aligned} \tag{50}$$

where $\boldsymbol{\Gamma}_{i,j} = \tau_2^{i-j} \prod_{k=j}^{i-1} \mathbf{S}_k$, $\tau_1 = \frac{1}{(1 - \alpha^2) \sigma_n^2}$, $\tau_2 = \alpha \tau_1$, and \mathcal{F} is defined in (20). Assuming all points in the constellation are transmitted with equal probability, the conditional probabilities in (50) are transformed by Baye's rule (a) and the Markovian property of channel (b, c), where these expressions can be obtained by iteratively synthesizing quadratic terms of \mathbf{h}_i , $i = 1, \dots, N_d$ in the exponents (d, e).

REFERENCES

- [1] G. Naik, J. Liu, and J.-M. J. Park, "Coexistence of wireless technologies in the 5 GHz bands: a survey of existing solutions and a roadmap for future research," *IEEE Commun. Surveys Tuts.*, vol. 20, no. 3, pp. 1777–1798, Mar. 2018.
- [2] N. Lee and R. W. Heath Jr, "Advanced interference management technique: Potentials and limitations," *IEEE Wireless Commun.*, vol. 23, no. 3, pp. 30–38, June 2016.
- [3] Samsung Electronics Co. Ltd., "5G vision," White paper, Aug. 2015.

- [4] Ericsson., "5G systems: Enabling the transportation of industry and society," Available at <https://www.ericsson.com/assets/local/publications/white-papers/wp-5g-systems.pdf> (Access on 2019/04/18), Jan. 2017.
- [5] S. A. A. Shah, E. Ahmed, M. Imran, and S. Zeadally, "5G for vehicular communications," *IEEE Commun. Mag.*, vol. 56, no. 1, pp. 111–117, Jan. 2018.
- [6] 3GPP, "Requirements for further advancements for evolved universal terrestrial radio access (E-UTRA) (LTE-Advanced)," Available at <https://www.3gpp.org/DynaReport/36913.htm>, July 2018.
- [7] J. Wu and P. Fan, "A survey on high mobility wireless communications: Challenges, opportunities and solutions," *IEEE Access*, vol. 4, pp. 450–476, Apr. 2016.
- [8] G. Noh, J. Kim, H. Chung, and I. Kim, "Realizing Multi-Gbps vehicular communication: Design, implementation, and validation," *IEEE Access*, vol. 7, pp. 19 435–19 446, Jan. 2019.
- [9] D. Bharadia, E. McMillin, and S. Katti, "Full duplex radios," in *Proc. ACM SIGCOMM Computer Commun. Rev.*, vol. 43, no. 4. ACM, 2013, pp. 375–386.
- [10] A. Sabharwal, P. Schniter, D. Guo, D. W. Bliss, S. Rangarajan, and R. Wichman, "In-band full-duplex wireless: Challenges and opportunities," *IEEE J. Sel. Areas Commun.*, vol. 32, no. 9, pp. 1637–1652, Sept. 2014.
- [11] E. Ahmed and A. M. Eltawil, "All-digital self-interference cancellation technique for full-duplex systems," *IEEE Trans. Wireless Commun.*, vol. 14, no. 7, pp. 3519–3532, July 2015.
- [12] D. Korpi, L. Anttila, V. Syrjälä, and M. Valkama, "Widely linear digital self-interference cancellation in direct-conversion full-duplex transceiver," *IEEE J. Sel. Areas Commun.*, vol. 32, no. 9, pp. 1674–1687, Sept. 2014.
- [13] M. T. Nguyen and L. B. Le, "Adjacent channel interference cancellation for robust spectrum sharing in satellite communications systems," in *Proc. IEEE PIMRC*, 2017, pp. 1–5.
- [14] V. Syrjälä, M. Valkama, L. Anttila, T. Riihonen, and D. Korpi, "Analysis of oscillator phase-noise effects on self-interference cancellation in full-duplex OFDM radio transceivers," *IEEE Trans. Wireless Commun.*, vol. 13, no. 6, pp. 2977–2990, June 2014.
- [15] E. Everett, A. Sahai, and A. Sabharwal, "Passive self-interference suppression for full-duplex infrastructure nodes," *IEEE Trans. Wireless Commun.*, vol. 13, no. 2, pp. 680–694, Feb. 2014.
- [16] M. Duarte, C. Dick, and A. Sabharwal, "Experiment-driven characterization of full-duplex wireless systems," *IEEE Trans. Wireless Commun.*, vol. 11, no. 12, pp. 4296–4307, Dec. 2012.
- [17] B. Debaillie, D.-J. van den Broek, C. Lavin, B. van Liempd, E. A. Klumperink, C. Palacios, J. Craninckx, B. Nauta, and A. Pärssinen, "Analog/RF solutions enabling compact full-duplex radios," *IEEE J. Sel. Areas Commun.*, vol. 32, no. 9, pp. 1662–1673, Sept. 2014.
- [18] K. Pedersen, G. Pocovi, J. Steiner, and A. Maeder, "Agile 5G scheduler for improved E2E performance and flexibility for different network implementations," *IEEE Commun. Mag.*, vol. 56, no. 3, pp. 210–217, Mar. 2018.
- [19] K. Schwarzenbarth, J. Grotz, and B. Ottersten, "MMSE based interference processing for satellite broadcast reception," in *Proc. IEEE VTC Spring*, 2007, pp. 1345–1349.
- [20] H. S. Wang and P.-C. Chang, "On verifying the first-order markovian assumption for a rayleigh fading channel model," *IEEE Trans. Veh. Technol.*, vol. 45, no. 2, pp. 353–357, May 1996.
- [21] S. Zhang, S.-C. Liew, and H. Wang, "Blind known interference cancellation," *IEEE J. Sel. Areas Commun.*, vol. 31, no. 8, pp. 1572–1582, Aug. 2013.
- [22] G. E. Bottomley and S. Chennakeshu, "Unification of MLSE receivers and extension to time-varying channels," *IEEE Trans. Commun.*, vol. 46, no. 4, pp. 464–472, Apr. 1998.
- [23] N. Sun and J. Wu, "Maximizing spectral efficiency for high mobility systems with imperfect channel state information," *IEEE Trans. Wireless Commun.*, vol. 13, no. 3, pp. 1462–1470, Mar. 2014.
- [24] X. Ma, G. B. Giannakis, and S. Ohno, "Optimal training for block transmissions over doubly selective wireless fading channels," *IEEE Trans. Signal Process.*, vol. 51, no. 5, pp. 1351–1366, May 2003.
- [25] Y. Zhu, D. Guo, and M. L. Honig, "A message-passing approach for joint channel estimation, interference mitigation, and decoding," *IEEE Trans. Wireless Commun.*, vol. 8, no. 12, Dec. 2009.
- [26] M. T. Nguyen and L. B. Le, "Channel estimation and symbol detection for communications on overlapping channels," in *IEEE Globecom Workshops (GC Wkshps)*, 2018, pp. 1–6.
- [27] C. C. Tan and N. C. Beaulieu, "On first-order markov modeling for the rayleigh fading channel," *IEEE Trans. Commun.*, vol. 48, no. 12, pp. 2032–2040, Dec. 2000.
- [28] Q. Fenzhong and Y. Liuqing, "On the estimation of doubly-selective fading channels," *IEEE Trans. Wireless Commun.*, vol. 9, no. 4, pp. 1261–1265, Apr. 2010.
- [29] T. Zemen and A. F. Molisch, "Adaptive reduced-rank estimation of nonstationary time-variant channels using subspace selection," *IEEE Trans. Veh. Technol.*, vol. 61, no. 9, pp. 4042–4056, Sept. 2012.
- [30] C. Xu, J. Zhang, T. Bai, P. Botsinis, R. G. Maunder, R. Zhang, and L. Hanzo, "Adaptive Coherent/Non-Coherent Single/Multiple-Antenna aided channel coded ground-to-air aeronautical communication," *IEEE Trans. Commun.*, vol. 67, no. 2, pp. 1099–1116, Feb. 2019.
- [31] A. Yeredor, "The joint MAP-ML criterion and its relation to ml and to extended least-squares," *IEEE Trans. Signal Process.*, vol. 48, no. 12, pp. 3484–3492, Dec. 2000.
- [32] L. Tong, B. M. Sadler, and M. Dong, "Pilot-assisted wireless transmissions: general model, design criteria, and signal processing," *IEEE Signal Process. Mag.*, vol. 21, no. 6, pp. 12–25, June 2004.
- [33] A. T. Asyhari and S. ten Brink, "Orthogonal or superimposed pilots? a rate-efficient channel estimation strategy for stationary MIMO fading channels," *IEEE Trans. Wireless Commun.*, vol. 16, no. 5, pp. 2776–2789, May 2017.
- [34] M. A. Mahamadu, J. Wu, Z. Ma, W. Zhou, Y. Tang, and P. Fan, "Fundamental tradeoff between doppler diversity and channel estimation errors in SIMO high mobility communication systems," *IEEE Access*, vol. 6, pp. 21 867–21 878, Apr. 2018.
- [35] R. G. Gallager, *Stochastic processes: theory for applications*. Cambridge University Press, 2013.